# EEG Channel Selection Using Gramian Angular Fields and Spectrograms for Energy Data Visualization

**Omer Faruk Kucukler [1,] *, Abbes Amira [2,1], Hossein Malekmohamadi [1]**

[1] *Institute of Artificial Intelligence, De Montfort University, Leicester, United Kingdom*
[2] *Department of Computer Science, University of Sharjah, Sharjah, United Arab Emirates*
***** *Corresponding author: p2611950@my365.dmu.ac.uk (O. F. Kucukler)*

**Abstract:** Electroencephalography (EEG)-based brain-computer interfaces (BCIs) have a wide range of applications in affect recognition. The usage of irrelevant information channels when decoding brain activity from different regions can negatively impact the task at hand. Therefore, further research is needed to determine the ideal channels for detecting superior performances. In this study, deep learning models and 2-D image representations are used to assess the efficacy of EEG channels for subjective valence responses to energy data visualizations. The EEG signals are converted into spectrograms and Gramian Angular Field (GAF) images. A hybrid Convolution Neural Network (CNN)-Long-Short Term Memory (LSTM) model and LSTM network are used to extract feature sets from the converted images. These feature sets, after reducing their dimensionality using a principal component analysis (PCA) method, are fed into a boosting classifier (AdaBoost). The performance metrics of both models and 2-D representations are compared. The LSTM and CNN-LSTM models with GAFs and spectrograms achieve state-of-the-art accuracies. The CNN-LSTM model achieves the highest performance when using spectrograms for the F8 channel, while the GAF method performs relatively lower for the F3 channel. The CNN-LSTM model with the spectrogram method produces reliable results, and hence, this method is used for further analysis of the remaining channel pairs. This study suggests that using a single EEG channel is more effective than using multiple channels for recognizing emotions in energy data visualizations. The proposed methodology is an efficient way to select channels for this purpose.

**Keywords:** deep learning; brain-computer interface; electroencephalography; energy; spectrogram; gramian angular field

## 1. Introduction

Electroencephalography (EEG) is a non-invasive technique for measuring electrical activity in the brain cortex (Alotaiby et al., 2015). EEG analysis has proven to be challenging due to its inherent complexity and difficulties in implementation. EEG measurement is facilitated by devices that use electrodes placed on the scalp to detect electrical activity. Many products are available on the market for non-invasive EEG applications, the most well-known of which are EMOTIV[1] and OpenBCI[2]. EEG capturing is a painless exploration of cerebral electrical activity that employs various electrode arrays of 8, 14, 32, and 256.

Klem et al. (1999) created an international 10-20 electrode placement system (Klem et al., 1999). This system is capable of detecting electrical activity in the frontal (F), parietal (P), occipital (O), and temporal (T) lobes. While there is no central lobe, central (C) is

[1] https://www.emotiv.com/epoc-flex/
[2] https://openbci.com/

designated as the central area. The brain cortex hemispheres are divided into even (right) and odd (left) groups. When contemplating these placements, a couple of inquiries may arise. It is crucial to extract useful features from EEG channels. Including irrelevant channels in the process results in acquiring superficial features, while incorporating channels not involved in cognitive tasks introduces noisy signals that negatively affect performance (Ghembaza and Djebbari, 2022; Mwata-Velu et al., 2022). In addition, EEG signals can be influenced by various disturbances such as noises and artefacts, including eye movements, blinks, and muscle activity on the face (Alarcão and Fonseca, 2019). EEG challenges have been addressed by researchers with various precautions and solutions. Researchers usually reduce the number of channels or features to reduce interference from irrelevant channels and complex characteristics and overfitting (Wang et al., 2019). Some researchers have even found that a single channel can represent the reaction of all channels (Joshi and B.Ghongade, 2020). The goal of reducing EEG electrodes for experiments is a widespread practice among researchers. Mwata Velu et al. (2022) emphasize that, while cognitive tasks are known to be associated with certain parts of the brain, the entire public EEG databases are collected via a variety of channels due to a lack of technological appropriation of devices (Mwata-Velu et al., 2022). Moreover, distinct regions of the brain are dedicated to particular functions, such as the frontal cortex being consistently associated with the recognition of emotions (Dennis and Solomon, 2010; Kober et al., 2008; Wagh and Vasanth, 2022). In this context, the objective of this paper is to design and validate a novel methodology for the selection of EEG channels by employing a unique 2-D image conversion technique and deep learning (DL) characteristics. An ensemble classifier is employed for the purpose of classifying valence emotion in the context of energy data visualization stimulus. The task of selecting energy data visualizations has been thoroughly evaluated within the framework of EEG channels. The EEG dataset has been generated and is now accessible to the public (Kucukler et al., 2024). The motivation for creating this dataset is to enhance energy users' behavior. Energy efficiency is a key objective of the United Nations' sustainable development goals. The behavior of energy users is a subtopic that addresses the excessive consumption of energy and aims to assist those who are still lacking access to energy. The purpose of this dataset is to analyze the preferences of energy users regarding data visualizations and provide them with the most appropriate visualization techniques to help them reduce their energy consumption. This approach can be incorporated into smart home systems to enhance device integration and minimize energy consumption through improved interaction.

In the field of EEG, neural networks are algorithms that have widespread applications (Gong et al., 2022). A recent study on depression detection utilizing EEGs employed CNN, LSTM, and BiLSTM models for EEG classification. The results indicate that the BiLSTM model outperforms the others, although all models demonstrate relatively exceptional performances (Gupta et al., 2024). The evaluation of EEG signals involves various techniques, and time-frequency representations obtained from these signals have proven to be effective. Researchers have implemented the Gramian Angular Field (GAF) image representation method to analyze load-carrying weight and posture in a dataset using a convolutional neural network- long-short-term memory (CNN-LSTM) model (Lee et al., 2020). Another study explored solar irradiation forecasting using a time-series Global Horizontal Irradiation (GHI) dataset, encoding time-series signals to GAF images and analyzing GAF images with a CNN-LSTM network (Hong et al., 2020). In an arrhythmia case analysis, researchers converted electrocardiography (ECG) signals to Hjorth parameters and encoded them to GAF images (Damaševičius et al., 2018). Meanwhile, a gas dataset containing Carbon monoxide and Ethylene gases was encoded to GAF images and used for gas classification with an AlexNet architecture (Jaleel et al., 2023). Spectrograms, on the other hand, are widely used techniques to learn spectral features of time-series data. They have been generated from EEG signals for

epileptic seizure detection (Ramos-Aguilar et al., 2020), brain balancing applications (Mustafa et al., 2020), and driver drowsiness detection analyses (Budak et al., 2019).

In this article, we present an analysis of EEG channels using time-frequency representations of EEG signals through spectrogram and GAF encoding. The resulting two-dimensional (2-D) images are evaluated using DL algorithms such as LSTM and CNN-LSTM to extract spectral features. Finally, a Boosting classifier is employed to analyze the features, and PCA is applied to reduce the dimensionality of the neural networks' output. The article's contributions are summarized as follows:

1) To implement a time-frequency encoding method for EEG signals using spectrograms and GAFs
2) To develop a novel feature extraction method from 2-D images using neural networks with GAF representations and spectrograms
3) To develop an EEG classification with valence emotion on energy data visualizations to benchmark EEG-channel analysis for emotion recognition.

The following sections of this paper are structured as follows: In Section 2, we will explore the existing literature on EEG analysis and channel selection techniques. Section 3 will cover the EEG data, data preprocessing, feature extraction, and classification model. We will present the outcome of our proposed approach in Section 4, along with our insights. Finally, we will conclude the paper in the last section.

## 2. Related Work

The examination of EEG channels in relation to task performance can be conducted in order to enhance the outcome of the analysis. This section provides an overview of recent significant advancements in the field of EEG signal channel selection and analysis, with a specific emphasis on 2-D representations and DL techniques. A summary of these contributions can be found in Table 1.

**Table 1.** EEG analyses made for different number of electrodes.

| Reference | Application | Database | Methods | Algorithms | Channels | Accuracy |
|---|---|---|---|---|---|---|
| **(Wang et al., 2019)** | EEG Emotion Recognition | DEAP | Normalized Mutual Information (NMI) | SVM | Valence (FC1, P3, Pz, Oz, CP2, C4, F4, and Fz) / Arousal (AF3, F7, FC5, P3, P7, Pz, O2, P4, FC6, and Fp2) | Valence - 74.41% / Arousal - 73.64% |
| **(Javidan et al., 2021)** | EEG-Emotion Recognition | DEAP | MSCE | SVR | F7, F8 | 67.45% |
| **(Joshi and B.Ghongade, 2020)** | EEG-Emotion Recognition | DEAP | Linear formulation of differential entropy | BiLSTM | Fp1 | 71.87% |
| **(Kumar G. S. et al., 2022)** | EEG-Emotion Recognition | DEAP | PSD | BiLSTM | Fp1, F3, F4, and Fp2 | Valence - 94.95% |
| **(Wagh and Vasanth, 2022)** | EEG-Emotion Recognition | SEED | Time and frequency domain features | DT | Fp1 and Fp2 | 71.52% |

| | | | | | | |
|---|---|---|---|---|---|---|
| **(Zhang et al., 2020)** | EEG-Emotion Recognition | DEAP | Raw EEG data | CNN-LSTM | 14 channels | 94.17% |
| **(Chen et al., 2021)** | EEG-Emotion Recognition | DEAP | Time, frequency domain features and nonlinear features | AdaBoost | 32 channels | Valence - 85.57% |
| **(Khan et al., 2022)** | EEG-Emotion Recognition | DREAMER | CNN features | XGBoost | 14 channels | Valence - 99.77% |

In their study, Wang et al. (2019) examined the effectiveness of EEG channels by utilizing normalized mutual information (NMI) to assess a subset of channels compared to all channels (Wang et al., 2019). The process involved generating spectrograms from EEG signals and then utilizing the NMI approach for a classification task of valence and arousal classes. The authors' findings indicated that the optimal number of channels for valence classes is eight, namely FC1, P3, Pz, Oz, CP2, C4, F4, and Fz, while arousal results showed ten channels, namely AF3, F7, FC5, P3, P7, Pz, O2, P4, FC6, and Fp2. Furthermore, the selected channels produced a valence accuracy of 74.41% and an arousal accuracy of 73.64%.

An analysis of EEG channels has shown that the F7 and F8 channels are effective for classifying positive and negative emotions using the DEAP dataset (Koelstra et al., 2012), employing the Magnitude Squared Coherence Estimate (MSCE) features, a Support Vector Regression (SVR) model achieved an accuracy of 67.45% (Javidan et al., 2021). On the other hand, a linear formulation of the differential entropy method produced an accuracy of 71.87% with a bi-directional long-short-term memory network (BiLSTM) for the Fp1 channel, which is comparable to the accuracy of all channels combined (Joshi and B.Ghongade, 2020). Kumar G. S. et al. (2022) compared machine learning classifiers such as K-nearest neighbour (KNN), Support Vector Machine (SVM), Artificial Neural Network (ANN), LSTM and BiLSTM models to determine the performance of EEG frontal channels (Fp1, F3, F4, and Fp2) in classifying positive and negative emotions at valence level (Kumar G. S. et al., 2022). The results showed that frontal channels performed better than all 32 channels with a BiLSTM classifier, achieving a 94.95% accuracy, which is 3.7% higher than the accuracy achieved by all channels. The authors of the study used Power Spectral Density (PSD) features for their analysis and suggested that monitoring channel-based behaviors using more distinct features could have implications for other EEG applications as well.

In their evaluation of 15 Chinese film clips, Wagh and Vasant (2022) utilized the SEED dataset (Zheng and Lu, 2015) to analyze positive, negative, and neutral emotions (Wagh and Vasanth, 2022). To accomplish this, they employed a discrete wavelet transform (DWT) technique that decomposed the EEG signal into frequency bands. The analysis utilized a combination of time-domain features and frequency features. The study compared channel pairs such as prefrontal (Fp1-Fp2), frontal (F3, F4), temporal (T3-T4), parietal (P7-P8), and occipital (O1-O2) using decision tree (DT) and KNN classifiers. Interestingly, Fp1 and Fp2 demonstrated superior accuracy of 71.52% with DT.

Zhang et al. (2020) conducted a thorough DL analysis of raw EEG signal and statistical feature data using various neural network models such as DNN, CNN, LSTM, and CNN-LSTM networks (Zhang et al., 2020). According to the results obtained from the DEAP dataset, the CNN and CNN-LSTM models performed better with raw EEG data, achieving accuracies of 90.12% and 94.17%, respectively. The authors selected 14 channels, including Fp1, AF3, F3,

F7, C3, P3, PO3, Fp2, AF4, F4, F8, C4, P4, and PO4, for the classification of valence and arousal classes. In a recent study by Chen et al. (2021), they introduced an ensemble classifier called AdaBoost to assess emotions of valence, arousal, dominance, and liking based on the DEAP dataset (Chen et al., 2021). The analysis involved combining time and frequency domain features with nonlinear domain features, followed by a linear discriminant analysis to reduce the feature set's dimensionality. The results showed an accuracy of 85.57% for valence using all channels with the AdaBoost architecture.

Khan et al. (2022) conducted a comparative study to monitor the affective states of participants while watching emotional video clips. They used the publicly available DREAMER dataset (Katsigiannis and Ramzan, 2018) and employed spectrogram images along with a fusion feature set to evaluate emotions related to valence, arousal, and dominance (Khan et al., 2022). Spectrograms were generated using Short-Time Fourier Transform (STFT), and CNN features were extracted from the spectrogram images from a dense layer. With the extracted CNN features, the Extreme Gradient Boosting (XGBoost) classifier achieved a performance of 99.71% for arousal, 99.77% for valence, and 99.77% for dominance. This prominent level of accuracy was made possible using 14 channels of data. In contrast, the feature fusion set, which included frequency-domain and statistical features, showed average accuracies of 95.17% for arousal, 87.46% for valence, and 84.54% for dominance with XGBoost classifier. On the other hand, GAF images have been used to classify epileptic seizures from EEG data using CNN architecture and accuracy of GAF images classification reached to 98%. (Shankar et al., 2020).

When examining the literature mentioned in this section, various feature sets and algorithms have been employed to analyze EEG emotion classification. CNN and LSTM algorithms have demonstrated superior performance compared to classical algorithms. Furthermore, the boosting classifier demonstrates superior performance when utilizing comparable features. Khan et al. (2022) demonstrated a noteworthy accomplishment by utilizing a CNN feature set extracted from spectrograms and employing a boosting classifier for classification, resulting in exceptional outcomes. Furthermore, GAF images have been scarcely utilized in conjunction with EEG signals, yet they have demonstrated exceptional efficacy in detecting seizures from EEG data. Nevertheless, they have yet to be employed for the purpose of emotion recognition. The utilization of feature extraction from GAF images has not been documented in existing literature. The utilization of GAF and spectrograms to extract DL features from EEG channels remains an intriguing approach for evaluating the method. Our investigation has uncovered that deep learning models, when combined with assessments based on literature and images, surpass EEG analyses in terms of effectiveness. For our study on analyzing the impact of energy data visualization, we employed spectrograms and GAF images with DL features to determine the most effective channel selection. This was achieved by training an AdaBoost classifier. The following section explores the chosen methodology, which draws inspiration from the literature on EEG channel analysis. It aims to demonstrate the significance of EEG channels in the process of emotion recognition. This methodology is evaluated using our openly accessible EEG dataset. This paper presents a novel application of GAF encoding for EEG emotion recognition. It includes a comparison with spectrograms and DL features. The classification of emotions for energy data visualizations is achieved by utilizing a novel combination of GAF and spectrogram features.

## 3. Methodology

This section includes the EEG database, EEG signal pre-processing, feature extraction, and classification phases.

*3.1 EEG database*

We conducted a study at De Montfort University where we collected an EEG database using energy data visualizations as stimuli. A total of 28 participants, comprising 23 males and 5 females aged between 19 and 48 years, took part in the experiments. To monitor the affective states of the participants, we used a popular EMOTIV Epoc Flex EEG kit with a 10-20 electrode system. The EEG signals were sampled at 128 Hz, and recordings were taken from Fp1, F7, F3, F4, F8, and Fp2 channels located in the frontal cortex, which is primarily associated with emotion elicitation (Alarcão and Fonseca, 2019; Suhaimi et al., 2020). During the experiments, we collected subjective responses from the participants through a self-assessment manikin (SAM) model, as presented in (Morris, 1995), to evaluate valence and arousal for each stimulus. In this study, we used valence to classify stimuli into high- and low-valence classes. The EEG dataset is available for researchers to validate their algorithms[3] (Kucukler et al., 2024).

*3.2 Pre-processing and feature extraction*

The analysis of EEG signals involves using two types of two-dimensional representation - spectrograms and Gramian Angular Fields (GAF). To extract deep learning features, a Long Short-Term Memory (LSTM) model and a CNN-LSTM model are employed on the 2D images. The flow diagram in Figure 1 outlines the method used. EEG signals are filtered with a band-pass filter between 0.5-60 Hz to obtain delta, theta, alpha, beta and gamma frequency bands. A 50 Hz notch filter is then employed to reduce electrical grid interference. The EEG dataset has a sampling rate of 128 Hz. The total number of samples for 28 participants and 10 data visualizations is 28 x 10 x 5040 for each channel, where each data visualization represents 5040 EEG samples. A sliding window technique is used to segment the pre-processed EEG signals into 20-second samples. From each sample, spectrograms and GAFs are produced with a 5-second overlap between windows. Segmenting EEG signals into windows serves the purpose of reducing computational load and speeding computation, while also enabling the extraction of additional features from each window's data. This process is carried out separately for each class data, subject, and channel. To reduce computational complexity and save time, the GAFs and spectrograms are transformed into grayscale images that have a uniform size of 640 x 480 pixels. After extracting features from 2-D representations using CNN-LSTM and LSTM models, we utilize the principal component analysis (PCA) technique to generate output. This output is then used as features for every channel with labels, consisting of ten components.

*3.2.1 Spectrogram*

A spectrogram is a visual representation of the changes in signal spectral density over time. The x-axis displays time while the y-axis displays frequency. Spectrograms are produced using the short-time Fourier transform (STFT):

$$STFT(x) = X(t,f) = \left|\sum_{t_1=0}^{N-1} x(t_1)h(t_1 - t)e^{-j2\pi f t_1}\right|^2 \quad (1)$$

where *x(t)* is the signal, *h(t)* is time window, N is the window size. This particular algorithm utilizes a process of segmenting the signal into smaller intervals and subsequently generates a periodogram for each of these intervals. The STFT pertains to the Fourier transform that is applied to these short-time segments. The method of STFT was employed to produce spectrograms of high resolution, measuring 640 x 480 pixels. It is noteworthy that a total of

[3] https://data.mendeley.com/datasets/w9nk4mvgbb

12522 spectrograms were successfully generated, considering the presence of 28 subjects, 6 channels, and 2 labels.

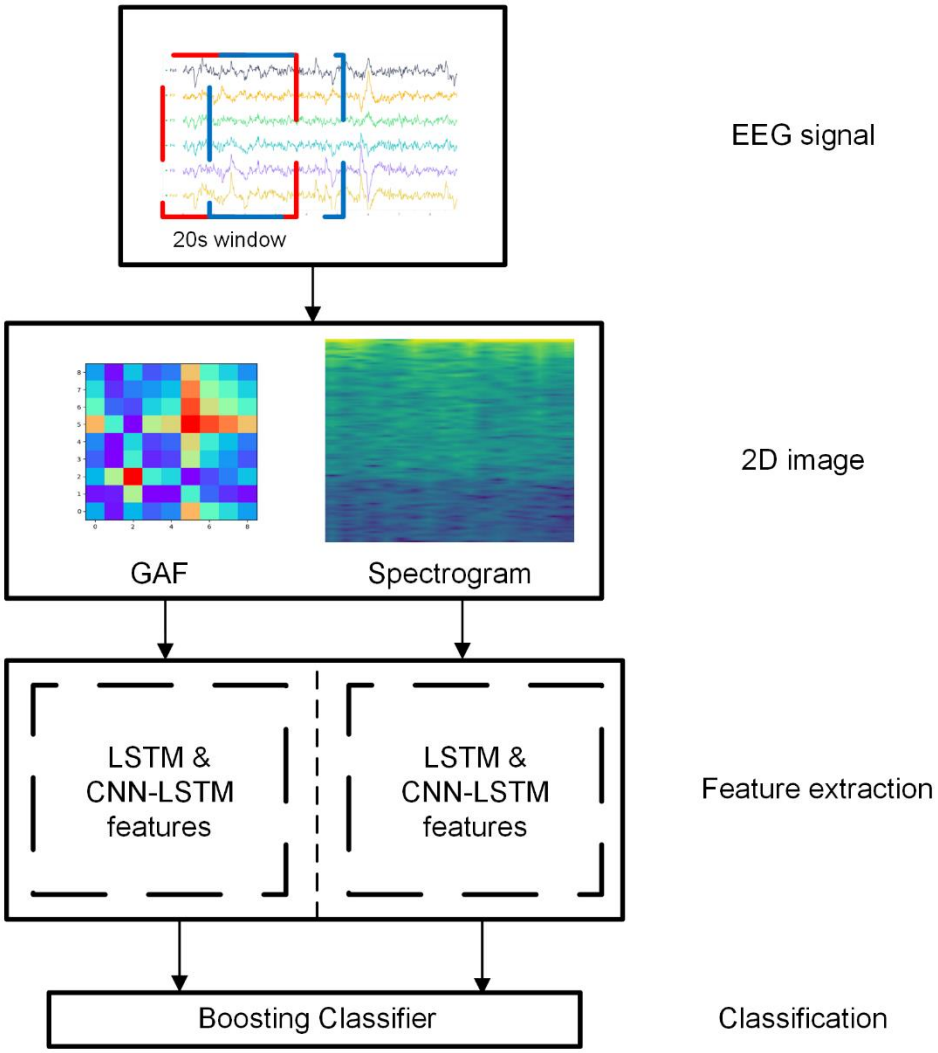


**Figure. 1.** Flow diagram of the classification of DL features from 2D images

*3.2.2 Gramian Angular Fields (GAFs)*

Gramian angular summation/difference fields (GASF/GADF) can be used to encode time series signals into 2D images using a polar coordinate conversion (Zhang et al., 2019). A time series signal $x = \{x_1, x_2, x_3, \dots, x_n\}$ is rescaled in the interval of [-1,1]:

$$resc(x_i) = \frac{(x_i - \max(x)) + (x_i - \min(x))}{\max(x) - \min(x)} \quad (2)$$

Since we created the rescaled *x* signal, now we can compute polar coordinates using the angular cosine of the signal and radius from the time stamp:

$$\begin{cases} \emptyset = arccos\big(resc(x_i)\big), -1 \le resc(x_i) \le 1, resc(x_i) \in resc(x) \\ r = \frac{t_i}{N}, t_i \in N \end{cases} \quad (3)$$

where $t_i$ is the time stamp and *N* is the constant factor. Following polar coordinate transformation, Gramian matrix (*G*) is defined as temporal correlations of each point using trigonometric summation or difference of angles as defined below:

$$GASF = G = \left[cos(\emptyset_i + \emptyset_j)\right] = \tilde{X}'.\tilde{X} - \sqrt{I - \tilde{X}'^2}.\sqrt{I - \tilde{X}^2} \quad (4)$$

$$GADF = G = \left[sin(\emptyset_i - \emptyset_j)\right] = \sqrt{I - \tilde{X}'^2}.\tilde{X} - \tilde{X}'.\sqrt{I - \tilde{X}^2} \quad (5)$$

where *I* is the unit row vector and *X'*, *X* are row vectors. In Figure 2, the formula for encoding time series signals into GAF images is shown. It is imperative to note that GAF images retain temporal information by preserving the correlation between angular directions and time as it increases, as emphasized by (Damaševičius et al., 2018; Wang and Oates, 2015; Zhang et al., 2019).

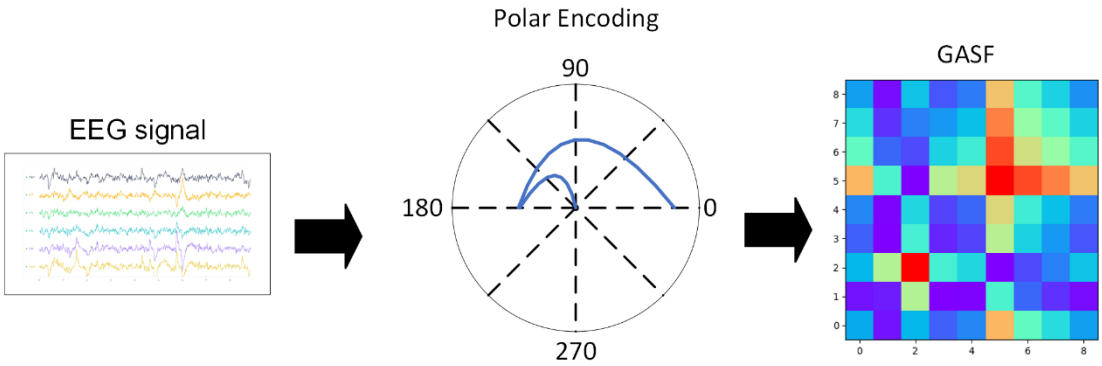


**Figure. 2.** Encoding time series signal into 2D GASF images

In this paper, GASF is employed using temporal connections for improved features for our EEG signals. The size of GAF images are 640 x 480 pixels and a total of 12522 GAF images for each channel are generated.

*3.2.3 Long short-term memory network*

Long short-term memory is a type of recurrent neural network that can deal with vanishing and exploding gradients (Xia et al., 2020). LSTM has the advantage of extracting features better than CNNs due to its memory cells. Memory cells expose the outputs of each hidden layer in terms of feature information (Qian et al., 2023). Memory cells have a significant impact on input, output, and forget gates. If the current input information is larger than the previous one, the memory is refreshed with new information, and the output gate decides whether or not to deliver the information. Figure 3 shows the structure of LSTM.

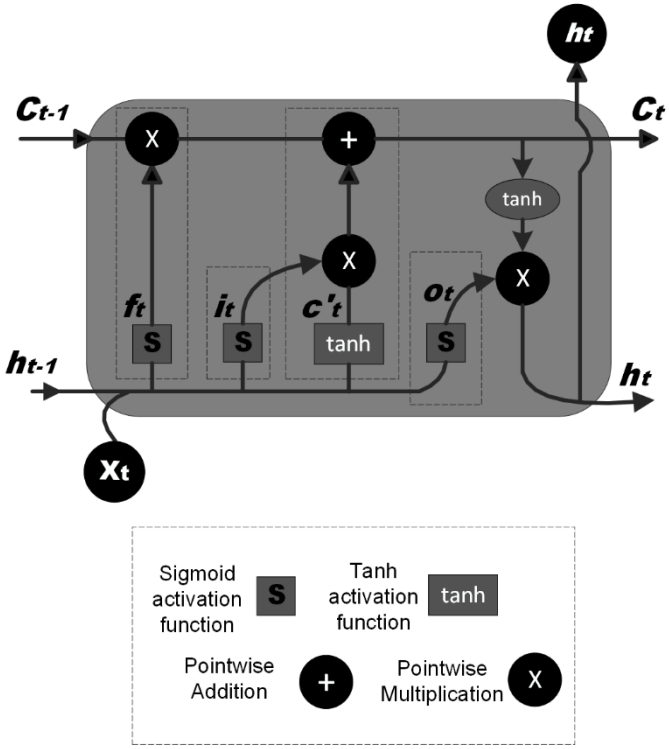


**Figure. 3.** LSTM structure

*3.2.4 CNN-LSTM network*

A Convolution Neural Network (CNN) comprises a convolution layer, max pooling layer, and fully connected layer that can effectively tackle the problem of overfitting while preserving the essential features of training samples (Bian et al., 2023). By using local receptive fields generated by a convolution kernel (Li et al., 2022), CNN can learn features from data without sacrificing any information. The convolution process of CNNs produces an output for input data X, which can be expressed as:

$$f_N(X) = \sum_{i=1}^{N} X_i * w_i + b_i \qquad (6)$$

where *N* is the convolution block, $X_i$ is the input. $w_i$ and $b_i$ represent weight and bias, respectively. " * " is the convolution product. The final convolution layer's output is fed into the fully connected layer for classification tasks.

In this research, we utilized a CNN with an LSTM layer to extract features from 2D images. The CNN-LSTM network structure is displayed in Figure 4, and it consists of a convolution layer, max pooling layer, convolution layer, max pooling layer, flatten layer, and LSTM layer. The LSTM layer's output is regarded as a feature vector for classification. The input size is (640,480). Convolution layers use Rectified Linear Unit (ReLU) activation, while tanh activation is employed for the LSTM layer. The flatten layer reduces dimensionality, and Table 2 displays the CNN-LSTM architecture's parameters along with LSTM. The first 2D convolution layer contains 64 filters and a 3 x 3 kernel size, followed by a 2D convolution layer with 128 filters and the same kernel size. After each convolution layer, a max-pooling layer is utilized to decrease feature size with a 2 x 2 pool size. A flatten layer is used before the LSTM layer to obtain a feature vector as an input for the LSTM layer, which consists of 128 filters. The adaptive moment estimation (ADAM) is selected as a loss function optimizer, with a

learning rate of 0.001. We trained the CNN-LSTM network under these settings to extract features.

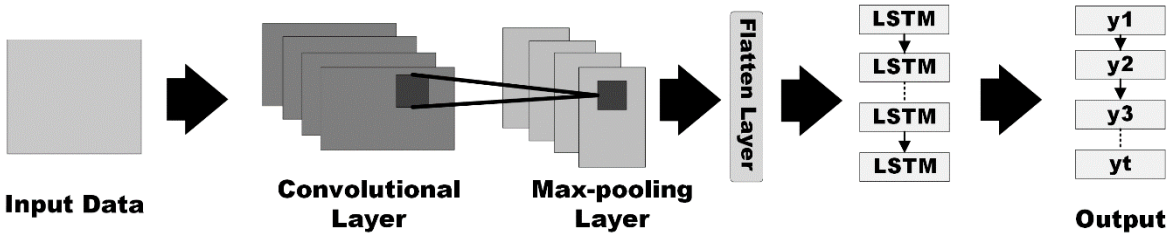


**Figure. 4.** CNN-LSTM architecture

*3.3 Classification*

Our research involves utilizing the AdaBoost ensemble classifier, also known as boosting classifier, on DL feature sets (Carrión-Ojeda et al., 2021; Chen et al., 2021). The adaptive nature of AdaBoost allows it to improve classification performance by increasing the weight of misclassified samples in the next training set. Furthermore, it has been shown to effectively address overfitting (Chen et al., 2021). Our implementation involves using the Decision Tree classifier as the estimator, with a PCA performed on the feature set to address overfitting issues (Subasi et al., 2021). The feature set is divided into two parts to carry out classification: 80% for training and 20% for testing. The GridSearchCV method is utilized to optimize the parameters of the AdaBoost classification model. Additionally, the principal component number for PCA is set to 10. The parameter grid for grid search consists of three values for the number of estimators (50, 100, 200), three values for the learning rate (0.1, 0.5, 1.0), and a cross-validation fold number of 5. The optimal parameters are utilized for training. Validation of the model is shown with metrics such as Accuracy, Sensitivity, Specificity, Mean Absolute Error(MAE), Root Mean Square Error (RMSE) and The coefficient of determination (R-squared). The metrics of evaluated performance are given as follows:

$$\text{Accuracy} = \frac{TN+TP}{TP+TN+FN+FP} \quad (7)$$

$$\text{Sensitivity} = \frac{TP}{TP+FN} \quad (8)$$

$$\text{Specificity} = \frac{TN}{TN+FP} \quad (9)$$

$$\text{MAE} = \frac{1}{N}\sum_{i=1}^{N}|y_i - \hat{y}| \quad (10)$$

$$\text{RMSE} = \sqrt{\frac{1}{N}\sum_{i=1}^{N}(y_i - \hat{y})^2} \quad (11)$$

$$\text{R-squared} = 1 - \frac{\sum(y_i-\hat{y})^2}{\sum(y_i-\bar{y})^2} \quad (12)$$

where TP represents the True-Positive class, TN shows the True-Negative class, FP shows the False-Positive, and FN represents the False-Negative class. $\hat{y}$ is the predicted value of y and $\bar{y}$ is the mean value of y. Accuracy is the percentage of instances classified correctly and It is the number of correct predictions divided by total predictions. The model's sensitivity is the percentage of positive instances correctly identified and calculated by dividing true positive

predictions by true positives and false negatives. Moreover, specificity is the percentage of negative instances the model correctly identifies and It equals true negative predictions divided by true negatives and false positives. Specificity complements sensitivity and is crucial for identifying negative incidents. On the other hand, MAE measures the average absolute difference between predicted and actual values. MAE simplifies prediction error interpretation and is less sensitive to outliers than RMSE. RMSE is the square root of the average squared differences between predicted and actual values and It is calculated as the square root of the average of squared errors (the sum of squared differences divided by the number of instances). RMSE measures prediction errors and is sensitive to large errors due to squaring. Lastly, R-squared measures how much of the target's variance is explained by the model's independent variables (features) and It equals 1 minus the model's sum of squared errors divided by the data's sum of squares. Higher R-squared values indicate a better model-data fit. If the model underperforms the average, it can be negative.

**Table 2.** Parameters of CNN-LSTM and LSTM architecture

| Architecture | Layer | Filters | Kernel | Activation |
|---|---|---|---|---|
| **CNN-LSTM** | Input | | | ReLU |
| | Conv2D | 64 | (3x3) | |
| | Max-Pooling | - | (2x2) | |
| | Conv2D | 128 | (3x3) | ReLU |
| | Max-Pooling | - | (2x2) | |
| | Flatten Layer | - | - | - |
| | LSTM | 128 | - | tanh |
| **LSTM** | LSTM | 32 | - | tanh |

## 4. Results and Discussion

In this section, we evaluate and discuss the outcomes of the provided approach. Six channels (Fp1, F7, F3, F4, F8, and Fp2) of collected EEG data are analyzed for affect recognition from energy data visualizations. Spectrograms and GAF images are generated from pre-processed EEG signals, and DL features are extracted from images for valence-level classification. Each channel's performance is evaluated, and comparisons of LSTM and CNN-LSTM methods for the optimal number of channels are investigated. A boosting classifier evaluates feature sets with an 80% training and 20% test split.

The proposed method evaluates the performance of each channel based on a classification task that distinguishes between high and low valence classes. Afterward, the performance of all possible channel pairs is analyzed. Reducing the number of channels not only simplifies data but also computational complexity (Wang et al., 2019). It is critical to determine which channel is best suited for a particular cognitive task. Additionally, the results obtained can assist researchers in studying with fewer sensors, thus reducing workload while still achieving accurate results. This study's findings shed light on how subsets of channels can be effectively utilized.

This research uses a Jupyter Notebook environment on Google Colaboratory (Intel® Xeon® CPU at 2.20 GHz) to calculate results. Using the LSTM with the GAF method, features are extracted from images on average in 0.074 s. On the other hand, the CNN-LSTM with the GAF method takes an average of 0.324 s per image. Meanwhile, using LSTM with spectrograms, the average time to extract features from each image is 0.089 s. Lastly, CNN-LSTM with spectrograms takes an average of 0.336 s per image to extract features.

Table 3 and Table 4 display the results of both LSTM and CNN-LSTM methods for GAF images across each channel. In addition, all tables include six performance metrics, including accuracy, sensitivity, specificity, MAE, RMSE, and R-squared. F7 achieved remarkable performance with the LSTM method, boasting 98.09% accuracy, 97.24% sensitivity, and 98.54% specificity. Meanwhile, the F3 channel outperformed the other channels with the CNN-LSTM method, with an impressive 99.76% accuracy, 99.31% sensitivity, and 100% specificity. The comparison between these techniques revealed that the F7 channel had the lowest accuracy with the CNN-LSTM method, but the highest accuracy with the LSTM method. This difference may have been caused by varying training data selections, leading to differing tolerance levels. However, F7 specificity improved with the CNN-LSTM approach. Overall, the CNN-LSTM method demonstrated superiority over the LSTM method in channel performance. These results indicate that the channels from the frontal cortex have a significant impact on the cognitive task of EEG, affirming the proposed method's effectiveness.

**Table 3.** GAF images performance metrics with LSTM features

| Channels | Accuracy (%) | Sensitivity (%) | Specificity (%) | MAE (%) | RMSE (%) | R^2 (%) |
|---|---|---|---|---|---|---|
| **Fp1** | 97.85 | 97.24 | 98.17 | 2.15 | 14.67 | 90.5 |
| **F7** | **98.09** | 97.24 | 98.54 | 1.91 | 13.83 | 91.55 |
| **F3** | 97.85 | 95.17 | 99.27 | 2.15 | 14.67 | 90.5 |
| **F4** | 94.74 | 91.67 | 96.35 | 5.26 | 22.94 | 76.69 |
| **F8** | 96.41 | 94.48 | 97.45 | 3.59 | 18.94 | 84.16 |
| **Fp2** | 96.65 | 97.24 | 96.34 | 3.35 | 18.3 | 85.22 |

Regarding Spectrogram analysis, the F3 channel extracted from LSTM features provided superior performance with an accuracy of 99.52%, sensitivity of 99.31% and specificity of 99.63%, as displayed in Table 5. In Table 6, the CNN-LSTM model showed impeccable performance with the F8 channel achieving 100% accuracy, sensitivity, and specificity. For EEG data, the CNN-LSTM method using Spectrogram representation displayed superior performance with an accuracy above 99.04% for all channels.

**Table 4.** GAF images performance metrics with CNN-LSTM features

| Channels | Accuracy (%) | Sensitivity (%) | Specificity (%) | MAE (%) | RMSE (%) | R^2 (%) |
|---|---|---|---|---|---|---|
| **Fp1** | 98.80 | 98.62 | 98.90 | 1.2 | 10.94 | 94.72 |
| **F7** | 97.85 | 95.86 | 98.90 | 2.15 | 14.67 | 90.5 |
| **F3** | **99.76** | 99.31 | 100 | 0.24 | 4.89 | 98.94 |
| **F4** | 98.09 | 94.44 | 100 | 1.91 | 13.83 | 91.53 |
| **F8** | 99.04 | 98.62 | 99.27 | 0.96 | 9.78 | 95.78 |
| **Fp2** | 99.52 | 98.62 | 100 | 0.48 | 6.92 | 97.89 |

In the field of literature, Javidan et al. (2021) utilized the Magnitude Squared Coherence Estimate (MSCE) technique in combination with a support vector regression

algorithm to analyze valence levels. Their study found that the F7-F8 channel pairs yielded the highest accuracy, reaching 67.5% (Javidan et al., 2021). Meanwhile, Kumar G. S. et al. (2022) reported that using the Fp1, F3, F4, and Fp2 frontal channels, along with a power spectral density feature set, and a Bi-LSTM model for valence and arousal classification, resulted in 94.95% accuracy, surpassing the accuracy of the 32 channel results at 92.15% (Kumar G. S. et al., 2022). In contrast, Wagh and Vasanth (2022) discovered that the Fp1 and Fp2 channels were optimal when utilizing time and frequency domain features to classify positive, negative, and neutral emotions (Wagh and Vasanth, 2022). Our method for predicting energy data visualization has been proven reliable through the use of frontal channels for valence classification, as evidenced by these findings.

**Table 5.** Spectrogram images performance metrics with LSTM features

| Channels | Accuracy (%) | Sensitivity (%) | Specificity (%) | MAE (%) | RMSE (%) | R^2 (%) |
|---|---|---|---|---|---|---|
| **Fp1** | 98.80 | 97.24 | 99.63 | 1.2 | 10.94 | 94.72 |
| **F7** | 94.98 | 91.04 | 97.07 | 5.02 | 22.41 | 77.83 |
| **F3** | **99.52** | 99.31 | 99.63 | 0.48 | 6.92 | 97.89 |
| **F4** | 99.28 | 98.68 | 99.62 | 0.72 | 8.48 | 96.89 |
| **F8** | 97.37 | 95.86 | 98.17 | 2.63 | 16.22 | 88.39 |
| **Fp2** | 99.28 | 98.62 | 99.63 | 0.72 | 8.47 | 96.83 |

In addition, we compared channel pairs using two methods and the results, displayed in Figure 5, were quite amusing. After analyzing all possible channel pairs, we found that the GAF-LSTM method had the worst performance, whereas the Spectrogram with the CNN-LSTM method had the best performance for all pairs. For instance, F4-Fp2 achieved an accuracy of 98.2% with Spectrogram with CNN-LSTM, while Fp1-F7 had the lowest performance with GAF-LSTM at only 85.87% accuracy. Furthermore, F3-Fp2 achieved high accuracy with both Spectrogram-LSTM and GAF with CNN-LSTM techniques, at 95.57% and 96.29% respectively.

**Table 6.** Spectrogram images performance metrics with CNN-LSTM features

| Channels | Accuracy (%) | Sensitivity (%) | Specificity (%) | MAE (%) | RMSE (%) | R^2 (%) |
|---|---|---|---|---|---|---|
| **Fp1** | 99.04 | 97.24 | 100 | 0.96 | 9.78 | 95.78 |
| **F7** | 99.28 | 97.93 | 100 | 0.72 | 8.47 | 96.83 |
| **F3** | 99.52 | 100 | 99.27 | 0.48 | 6.92 | 97.89 |
| **F4** | 99.76 | 100 | 99.62 | 0.24 | 4.9 | 98.97 |
| **F8** | **100** | 100 | 100 | 0 | 0 | 100 |
| **Fp2** | 99.52 | 98.62 | 100 | 0.48 | 6.92 | 97.89 |

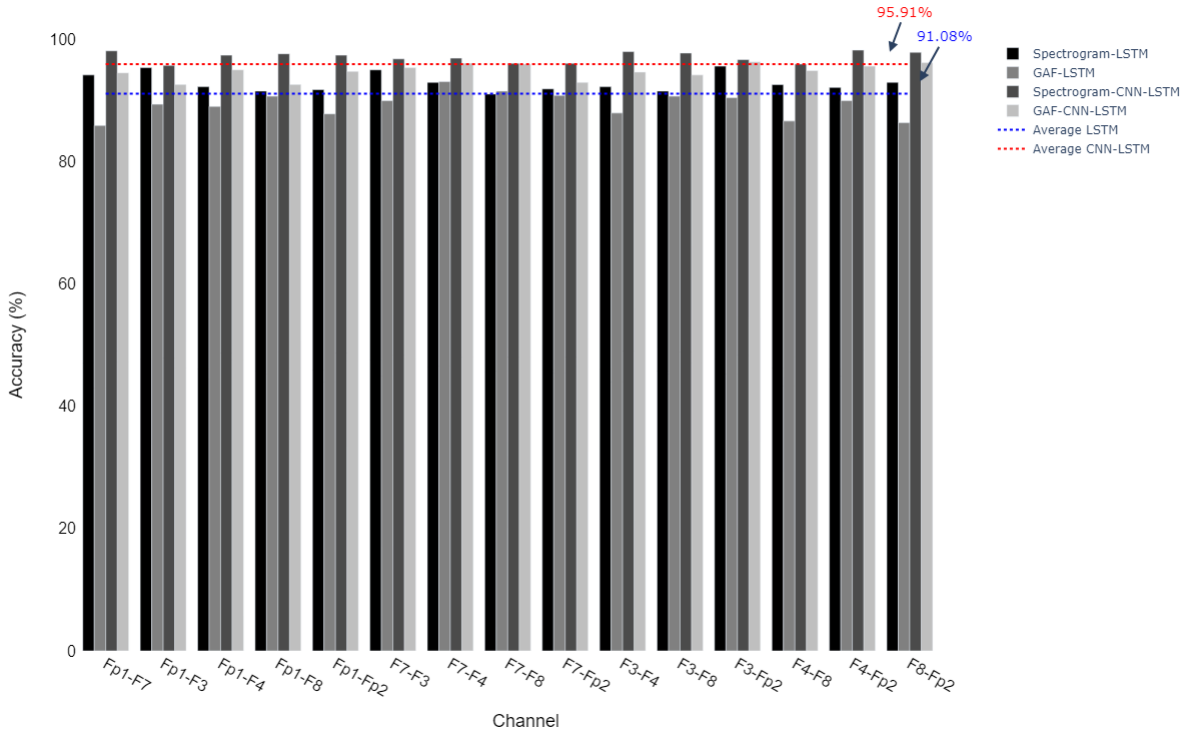


**Figure. 5.** Comparison of classification accuracies with channel pairs

As an alternative approach, we utilized the eXtreme Gradient Boosting (XGBoost) classifier and conducted a comparison with AdaBoost for each channel. Figure 6 displays the outcomes for both images and features. XGBoost consistently outperforms AdaBoost in terms of accuracy across all architectures and features. Based on consistent performance superiority, XGBoost appears to be a more favorable choice compared to AdaBoost in this particular context. Spectrograms exhibit superior performance compared to GAFs in all architectures. Notably, spectrograms with CNN-LSTM features achieved the highest level of performance. Although GAFs yield valuable results, they appear to be less efficient compared to spectrograms.

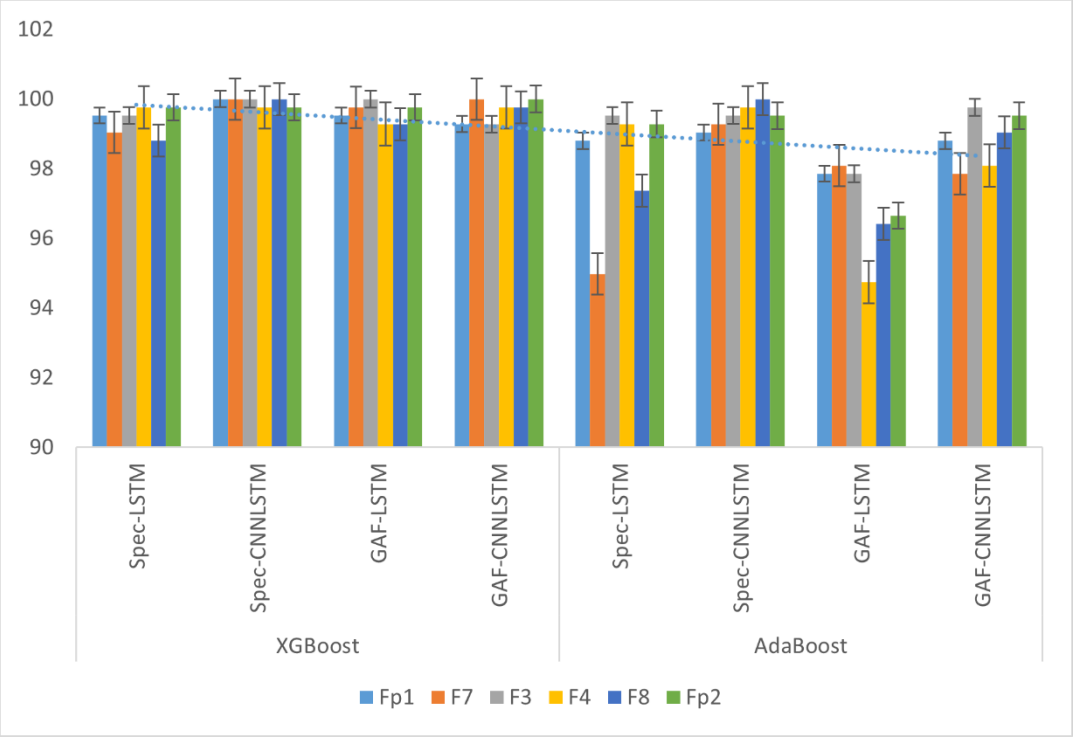


**Figure. 6.** Comparison of classifiers for each channel

Furthermore, the performance of the model is assessed for various train-test splits. Tables 7 and 8 display the precise accuracies for each channel in both the images and features. The train-test splits are 60%-40%, 70%-30%, 80%-20%, and 90%-10%, respectively. The model consistently demonstrates high performance across various splits, with average accuracies ranging from approximately 97.35% to 99.6% for spectrograms and 96.75% to 99.28% for GAFs.

**Table 7.** Spectrogram images accuracies with LSTM and CNN-LSTM for different train-test splits

| Channels | LSTM (%) | | | | CNN-LSTM (%) | | | |
|---|---|---|---|---|---|---|---|---|
| | 60-40 | 70-30 | 80-20 | 90-10 | 60-40 | 70-30 | 80-20 | 90-10 |
| **Fp1** | 97.25 | 98.57 | 98.57 | 99.04 | 99.16 | 99.04 | 99.04 | 100 |
| **F7** | 94.14 | 95.21 | 95.93 | 97.13 | 98.2 | 98.41 | 99.04 | 99.52 |
| **F3** | 99.16 | 99.36 | 99.52 | 98.57 | 99.88 | 99.36 | 99.76 | 99.52 |
| **F4** | 98.2 | 98.88 | 99.28 | 99.04 | 99.16 | 99.68 | 99.76 | 99.52 |
| **F8** | 97.37 | 97.13 | 97.61 | 98.57 | 99.88 | 99.84 | 100 | 100 |
| **Fp2** | 97.96 | 97.93 | 99.52 | 99.52 | 99.16 | 99.36 | 99.52 | 99.04 |
| **Average** | **97.35** | **97.85** | **98.41** | **98.65** | **99.24** | **99.28** | **99.52** | **99.6** |

**Table 8.** GAF images accuracies with LSTM and CNN-LSTM for different train-test splits

| Channels | LSTM (%) | | | | CNN-LSTM (%) | | | |
|---|---|---|---|---|---|---|---|---|
| | 60-40 | 70-30 | 80-20 | 90-10 | 60-40 | 70-30 | 80-20 | 90-10 |
| **Fp1** | 97.25 | 97.93 | 96.89 | 97.61 | 99.16 | 99.2 | 98.57 | 99.04 |
| **F7** | 97.25 | 97.77 | 97.85 | 99.52 | 97.49 | 97.61 | 98.8 | 99.52 |
| **F3** | 98.56 | 97.93 | 98.09 | 99.52 | 99.64 | 99.04 | 98.57 | 99.52 |
| **F4** | 94.62 | 94.26 | 94.02 | 95.22 | 98.57 | 98.41 | 97.85 | 98.57 |
| **F8** | 95.81 | 97.45 | 96.41 | 98.09 | 97.13 | 98.73 | 99.04 | 99.52 |

| | | | | | | | | |
|---|---|---|---|---|---|---|---|---|
| **Fp2** | 97.01 | 96.65 | 96.17 | 96.65 | 98.92 | 99.2 | 99.28 | 99.52 |
| **Average** | **96.75** | **97** | **96.57** | **97.77** | **98.49** | **98.7** | **98.69** | **99.28** |

Additionally, an innovative idea is introduced by combining GAF and spectrogram images to extract LSTM and CNN-LSTM features, as presented in Tables 9 and 10. The results showed that the CNN-LSTM features outperformed the other fused features, achieving an accuracy of 98.2% with the F3 channel. When compared to previous results, CNN-LSTM demonstrated comparable performance to fused features, particularly in the F3 and F8 channels where it showed superior performance. The LSTM model achieved the highest accuracy when using fused features from the F4 channel, as opposed to the F7 and F3 channels achieved the highest in previous LSTM feature performances. Furthermore, the fusion of channels resulted in a decrease in overall accuracies.

**Table 9.** Fused GAF and spectrogram LSTM features performance

| Channels | Accuracy (%) | Sensitivity (%) | Specificity (%) | MAE (%) | RMSE (%) | R^2 (%) |
|---|---|---|---|---|---|---|
| **Fp1** | 90.18 | 79.87 | 95.9 | 09.82 | 31.34 | 57.21 |
| **F7** | 89.94 | 88.26 | 90.88 | 10.06 | 31.72 | 56.17 |
| **F3** | 92.58 | 84.9 | 96.83 | 07.43 | 27.25 | 67.65 |
| **F4** | **92.93** | 91.97 | 93.47 | 07.07 | 26.58 | 69.26 |
| **F8** | 90.66 | 80.54 | 96.28 | 09.34 | 30.56 | 59.3 |
| **Fp2** | 90.54 | 84.23 | 94.04 | 09.46 | 30.76 | 58.78 |

**Table 10.** Fused GAF and spectrogram CNN-LSTM features performance

| Channels | Accuracy (%) | Sensitivity (%) | Specificity (%) | MAE (%) | RMSE (%) | R^2 (%) |
|---|---|---|---|---|---|---|
| **Fp1** | 94.01 | 92.95 | 94.6 | 05.99 | 24.47 | 73.91 |
| **F7** | 94.85 | 92.62 | 96.09 | 05.15 | 22.69 | 77.56 |
| **F3** | **98.2** | 96.98 | 98.88 | 01.8 | 13.4 | 92.17 |
| **F4** | 93.05 | 87.96 | 95.9 | 06.95 | 26.36 | 69.78 |
| **F8** | 96.17 | 94.63 | 97.02 | 03.83 | 19.58 | 83.3 |
| **Fp2** | 95.33 | 93.29 | 96.46 | 04.67 | 21.61 | 79.65 |

Our study focused on analyzing the performance of EEG data channels in participants who were stimulated by energy data visualizations. We collected subjective responses on the valence scale for different graphs. We generated two types of 2-D image representations of EEG signals: Spectrograms and GAFs. We extracted DL features from these 2-D images for the classification task and used a Boosting classifier to obtain the classification results. We evaluated channel pair performances as well as each channel's achievements. To validate the proposed approach's performance, we used different metrics. We compared two feature extraction methods, LSTM and CNN-LSTM, to determine their reliability in displaying EEG patterns with the applied task. Our results showed that Spectrograms outperformed GAFs, and CNN-LSTM was more powerful in presenting EEG characteristics. We demonstrated that 2-D image representation provides a useful method for mapping intrinsic EEG channel behavior for affect recognition tasks.

Based on the results, we investigate the performance differences for the remaining channel pairs, which include pairs with 3 channels, 4 channels, 5 channels, and 6 channels. CNN-LSTM with spectrogram is chosen to analyze the performance of pairs. Table 11 shows the results for channel pairs. According to the analysis results, Fp1-F8-Fp2 channels achieve

the highest accuracy of 94.57% among this group, while all channels achieve the lowest accuracy of 81.11%. An increase in channels results in decreased performance, as shown in Figure 7 with average accuracy. This result demonstrates the researchers' point that using more channels increases the complexity of analysis and yields poor results (Ghembaza and Djebbari, 2022; Joshi and B.Ghongade, 2020). This finding highlights the fact that as the number of channels increases, CNN-LSTM models with spectrograms become less accurate.

**Table 11** Comparison of performance metrics for possible channel pairs

| Channel | Accuracy (%) | Sensitivity (%) | Specificity (%) | MAE (%) | RMSE (%) | R^2 (%) | Pair |
|---|---|---|---|---|---|---|---|
| **Fp1-F7-F3** | 93.93 | 92.21 | 94.91 | 6.07 | 24.63 | 73.63 | 3-ch |
| **Fp1-F7-F4** | 90.89 | 88.2 | 92.41 | 9.11 | 30.18 | 60.42 | 3-ch |
| **Fp1-F7-F8** | 91.22 | 85.08 | 94.66 | 8.78 | 29.63 | 61.82 | 3-ch |
| **Fp1-F7-Fp2** | 92.42 | 88.2 | 94.78 | 7.59 | 27.54 | 67.03 | 3-ch |
| **Fp1-F3-F4** | 92.65 | 89.76 | 94.28 | 7.35 | 27.11 | 68.06 | 3-ch |
| **Fp1-F3-F8** | 92.9 | 90.43 | 94.28 | 7.11 | 26.66 | 69.11 | 3-ch |
| **Fp1-F3-Fp2** | 91.06 | 85.75 | 94.03 | 8.94 | 29.9 | 61.13 | 3-ch |
| **Fp1-F4-F8** | 94.17 | 92.3 | 95.24 | 5.84 | 24.15 | 74.78 | 3-ch |
| **Fp1-F4-Fp2** | 92.25 | 89.21 | 93.99 | 7.75 | 27.84 | 66.48 | 3-ch |
| **Fp1-F8-Fp2** | **94.57** | 90.43 | 96.9 | 5.43 | 23.3 | 76.4 | 3-ch |
| **F7-F3-F4** | 91.37 | 89.09 | 92.66 | 8.63 | 29.38 | 62.5 | 3-ch |
| **F7-F3-F8** | 92.1 | 89.31 | 93.66 | 7.91 | 28.11 | 65.64 | 3-ch |
| **F7-F3-Fp2** | 91.54 | 85.31 | 95.03 | 8.46 | 29.09 | 63.21 | 3-ch |
| **F7-F4-F8** | 87.86 | 81.5 | 91.48 | 12.15 | 34.85 | 47.48 | 3-ch |
| **F7-F4-Fp2** | 88.58 | 82.6 | 91.98 | 11.43 | 33.8 | 50.59 | 3-ch |
| **F7-F8-Fp2** | 89.47 | 80.85 | 94.28 | 10.54 | 32.46 | 54.19 | 3-ch |
| **F3-F4-F8** | 89.94 | 84.81 | 92.86 | 10.07 | 31.73 | 56.46 | 3-ch |
| **F3-F4-Fp2** | 90.89 | 83.71 | 94.99 | 9.11 | 30.18 | 60.61 | 3-ch |
| **F3-F8-Fp2** | 91.7 | 83.75 | 96.15 | 8.31 | 28.81 | 63.91 | 3-ch |
| **F4-F8-Fp2** | 91.53 | 86 | 94.64 | 8.47 | 29.1 | 63.23 | 3-ch |
| **Fp1-F7-F3-F4** | 89.04 | 82.26 | 92.71 | 10.97 | 33.12 | 51.88 | 4-ch |
| **Fp1-F7-F3-F8** | 88.26 | 81.22 | 91.97 | 11.74 | 34.26 | 48.02 | 4-ch |
| **Fp1-F7-F3-Fp2** | 89.7 | 84.53 | 92.43 | 10.3 | 32.1 | 54.38 | 4-ch |
| **Fp1-F7-F4-F8** | 85.02 | 75.26 | 90.2 | 14.98 | 38.71 | 33.84 | 4-ch |
| **Fp1-F7-F4-Fp2** | 92.15 | 86.68 | 95.06 | 7.85 | 28.02 | 65.33 | 4-ch |
| **Fp1-F7-F8-Fp2** | 87.6 | 82.79 | 90.14 | 12.4 | 35.21 | 45.1 | 4-ch |
| **Fp1-F3-F4-F8** | 88.32 | 83.74 | 90.75 | 11.69 | 34.19 | 48.39 | 4-ch |
| **Fp1-F3-F4-Fp2** | 88.74 | 82.7 | 91.94 | 11.27 | 33.57 | 50.25 | 4-ch |
| **Fp1-F3-F8-Fp2** | 88.98 | 82.27 | 92.52 | 11.02 | 33.2 | 51.2 | 4-ch |
| **Fp1-F4-F8-Fp2** | 86.82 | 77.11 | 92.01 | 13.19 | 36.31 | 41.92 | 4-ch |
| **F7-F3-F4-F8** | 85.08 | 75.26 | 90.29 | 14.92 | 38.63 | 34.1 | 4-ch |
| **F7-F3-F4-Fp2** | 89.51 | 80.97 | 94.05 | 10.49 | 32.39 | 53.69 | 4-ch |
| **F7-F3-F8-Fp2** | 88.38 | 78.61 | 93.52 | 11.62 | 34.09 | 48.55 | 4-ch |
| **F7-F4-F8-Fp2** | 88.68 | 78.49 | 94.12 | 11.33 | 33.66 | 50.1 | 4-ch |
| **F3-F4-F8-Fp2** | 87.48 | 78.66 | 92.19 | 12.53 | 35.39 | 44.82 | 4-ch |
| **Fp1-F7-F3-F4-F8** | 85.82 | 75.69 | 91.3 | 14.19 | 37.67 | 37.72 | 5-ch |
| **Fp1-F7-F3-F4-Fp2** | 84.81 | 75.82 | 89.67 | 15.19 | 38.98 | 33.3 | 5-ch |
| **Fp1-F7-F3-F8-Fp2** | 84.48 | 75.98 | 89.16 | 15.53 | 39.41 | 32.21 | 5-ch |

| | | | | | | | |
|---|---|---|---|---|---|---|---|
| **Fp1-F7-F4-F8-Fp2** | 85.53 | 75.86 | 90.73 | 14.48 | 38.05 | 36.34 | 5-ch |
| **Fp1-F3-F4-F8-Fp2** | 84.04 | 74.49 | 89.18 | 15.96 | 39.95 | 29.8 | 5-ch |
| **F7-F3-F4-F8-Fp2** | 84.09 | 73.8 | 89.62 | 15.91 | 39.89 | 30.02 | 5-ch |
| **Fp1-F7-F3-F4-F8-Fp2** | 81.11 | 66.15 | 89.48 | 18.89 | 43.47 | 17.88 | 6-ch |

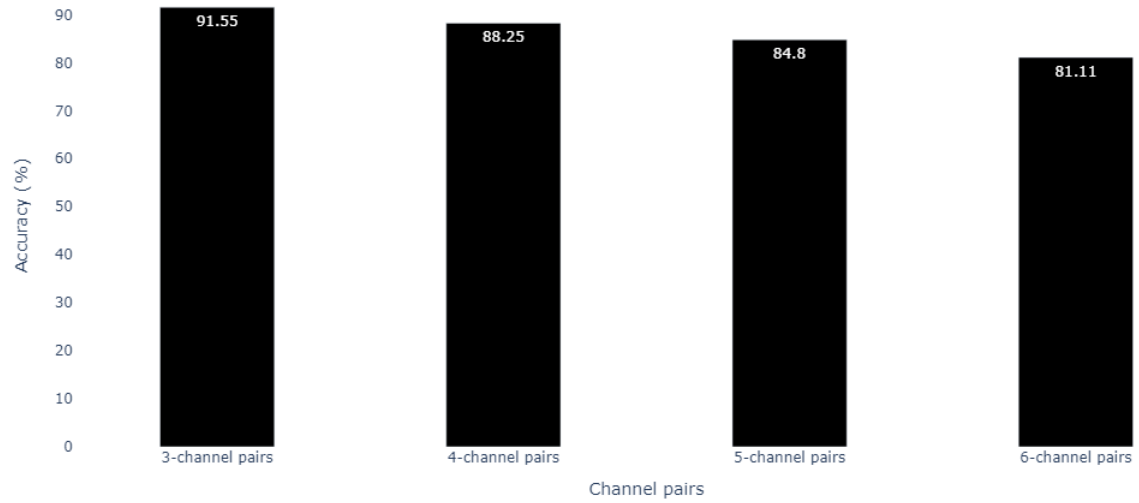


**Figure. 7.** Comparison of average classification accuracies for channel pairs

## 5. Conclusions

In this article, a method for selecting EEG channels to recognize the affect in energy data visualizations is proposed. A database of collected EEGs was used to compare LSTM and CNN-LSTM features extracted from 2-D GAFs and spectrograms using an AdaBoost classifier. The investigation was conducted with pairs of models and 2-D representations using a cloud-based architecture. Pre-processed signals were segmented into 20-second windows and spectrograms and GAFs were generated for each window data. The current results showed that CNN-LSTM features and the spectrogram method achieved a maximum accuracy of 100% with the F8 channel, while the F4-Fp2 channel pair achieved an accuracy of 98.2% with CNN-LSTM and the spectrogram method. In addition, we selected the most reliable model and methodology in our study to evaluate methodological consistency for all possible channel pairs. The findings indicated that as the number of channels increases, accuracy decreases, revealing an inverse correlation between the number of channels and classification performance. Our future works will involve exploring the arousal dimension to compare the outcomes of this study and implementing robust techniques to enhance overall channel performance.

## Credit author statement

**Omer Faruk Kucukler**: Conceptualization, Methodology, Software, Validation, Data curation, Visualization, Writing—original draft preparation, Writing—review and editing **Abbes Amira**: Supervision, Writing—review and editing **Hossein Malekmohamadi**: Supervision, Writing—

review and editing. All authors have read and agreed to the published version of the manuscript.

## References


Alarcão, S.M., Fonseca, M.J., 2019. Emotions Recognition Using EEG Signals: A Survey. IEEE Transactions on Affective Computing 10, 374–393. https://doi.org/10.1109/TAFFC.2017.2714671

Alotaiby, T., El-Samie, F.E.A., Alshebeili, S.A., Ahmad, I., 2015. A review of channel selection algorithms for EEG signal processing. EURASIP J. Adv. Signal Process. 2015, 66. https://doi.org/10.1186/s13634-015-0251-9

Bian, S., Wang, Z., Song, W., Zhou, X., 2023. Feature extraction and classification of time-varying power load characteristics based on PCANet and CNN+Bi-LSTM algorithms. Electric Power Systems Research 217, 109149. https://doi.org/10.1016/j.epsr.2023.109149

Budak, U., Bajaj, V., Akbulut, Y., Atila, O., Sengur, A., 2019. An Effective Hybrid Model for EEG-Based Drowsiness Detection. IEEE Sensors Journal 19, 7624–7631. https://doi.org/10.1109/JSEN.2019.2917850

Carrión-Ojeda, D., Fonseca-Delgado, R., Pineda, I., 2021. Analysis of factors that influence the performance of biometric systems based on EEG signals. Expert Systems with Applications 165, 113967. https://doi.org/10.1016/j.eswa.2020.113967

Chen, Y., Chang, R., Guo, J., 2021. Emotion Recognition of EEG Signals Based on the Ensemble Learning Method: AdaBoost. Mathematical Problems in Engineering 2021, e8896062. https://doi.org/10.1155/2021/8896062

Damaševičius, R., Maskeliūnas, R., Woźniak, M., Połap, D., 2018. Visualization of physiologic signals based on Hjorth parameters and Gramian Angular Fields, in: 2018 IEEE 16th World Symposium on Applied Machine Intelligence and Informatics (SAMI). Presented at the 2018 IEEE 16th World Symposium on Applied Machine Intelligence and Informatics (SAMI), pp. 000091–000096. https://doi.org/10.1109/SAMI.2018.8323992

Dennis, T.A., Solomon, B., 2010. Frontal EEG and Emotion Regulation: Electrocortical Activity in Response to Emotional Film Clips is Associated with Reduced Mood Induction and Attention Interference Effects. Biol Psychol 85, 456–464. https://doi.org/10.1016/j.biopsycho.2010.09.008

Ghembaza, F., Djebbari, A., 2022. A Robust Dynamic EEG Channel Selection using Time–Frequency Extended Renyi Entropy, in: 2022 7th International Conference on Image and Signal Processing and Their Applications (ISPA). Presented at the 2022 7th International Conference on Image and Signal Processing and their Applications (ISPA), pp. 1–8. https://doi.org/10.1109/ISPA54004.2022.9786317

Gong, S., Xing, K., Cichocki, A., Li, J., 2022. Deep Learning in EEG: Advance of the Last Ten-Year Critical Period. IEEE Transactions on Cognitive and Developmental Systems 14, 348–365. https://doi.org/10.1109/TCDS.2021.3079712

Gupta, C., Khullar, V., Goyal, N., Saini, K., Baniwal, R., Kumar, S., Rastogi, R., 2024. Cross-Silo, Privacy-Preserving, and Lightweight Federated Multimodal System for the Identification of Major Depressive Disorder Using Audio and Electroencephalogram. Diagnostics 14, 43. https://doi.org/10.3390/diagnostics14010043

Hong, Y.-Y., Martinez, J.J.F., Fajardo, A.C., 2020. Day-Ahead Solar Irradiation Forecasting Utilizing Gramian Angular Field and Convolutional Long Short-Term Memory. IEEE Access 8, 18741–18753. https://doi.org/10.1109/ACCESS.2020.2967900

Jaleel, M., Kucukler, O.F., Alsalemi, A., Amira, A., Malekmohamadi, H., Diao, K., 2023. Analyzing Gas Data Using Deep Learning and 2-D Gramian Angular Fields. IEEE Sensors Journal 23, 6109–6116. https://doi.org/10.1109/JSEN.2023.3243149

Javidan, M., Yazdchi, M., Baharlouei, Z., Mahnam, A., 2021. Feature and channel selection for designing a regression-based continuous-variable emotion recognition system with two EEG channels. Biomedical Signal Processing and Control 70, 102979. https://doi.org/10.1016/j.bspc.2021.102979

Joshi, V.M., B.Ghongade, R., 2020. Optimal Number of Electrode Selection for EEG Based Emotion Recognition using Linear Formulation of Differential Entropy. Biomedical and Pharmacology Journal 13, 645–653.

Katsigiannis, S., Ramzan, N., 2018. DREAMER: A Database for Emotion Recognition Through EEG and ECG Signals From Wireless Low-cost Off-the-Shelf Devices. IEEE Journal of Biomedical and Health Informatics 22, 98–107. https://doi.org/10.1109/JBHI.2017.2688239

Khan, M.S., Salsabil, N., Alam, M.G.R., Dewan, M.A.A., Uddin, M.Z., 2022. CNN-XGBoost fusion-based affective state recognition using EEG spectrogram image analysis. Sci Rep 12, 14122. https://doi.org/10.1038/s41598-022-18257-x

Klem, G., Lüders, H., Jasper, H., Elger, C., 1999. The ten-twenty electrode system of the International Federation. The International Federation of Clinical Neurophysiology. Electroencephalography and clinical neurophysiology. Supplement.

Kober, H., Barrett, L.F., Joseph, J., Bliss-Moreau, E., Lindquist, K., Wager, T.D., 2008. Functional grouping and cortical–subcortical interactions in emotion: A meta-analysis of neuroimaging studies. NeuroImage 42, 998–1031. https://doi.org/10.1016/j.neuroimage.2008.03.059

Koelstra, S., Muhl, C., Soleymani, M., Lee, J.-S., Yazdani, A., Ebrahimi, T., Pun, T., Nijholt, A., Patras, I., 2012. DEAP: A Database for Emotion Analysis ;Using Physiological Signals. IEEE Transactions on Affective Computing 3, 18–31. https://doi.org/10.1109/T-AFFC.2011.15

Kucukler, O.F., Amira, A., Malekmohamadi, H., 2024. EEG dataset for energy data visualizations. Data in Brief 52, 109933. https://doi.org/10.1016/j.dib.2023.109933

Kumar G. S., S., Arun, A., Sampathila, N., Vinoth, R., 2022. Machine Learning Models for Classification of Human Emotions Using Multivariate Brain Signals. Computers 11, 152. https://doi.org/10.3390/computers11100152

Lee, H., Yang, K., Kim, N., Ahn, C.R., 2020. Detecting excessive load-carrying tasks using a deep learning network with a Gramian Angular Field. Automation in Construction 120, 103390. https://doi.org/10.1016/j.autcon.2020.103390

Li, H., Ding, M., Zhang, R., Xiu, C., 2022. Motor imagery EEG classification algorithm based on CNN-LSTM feature fusion network. Biomedical Signal Processing and Control 72, 103342. https://doi.org/10.1016/j.bspc.2021.103342

Morris, J.D., 1995. Observations: SAM: The self-assessment manikin: An efficient cross-cultural measurement of emotional response. Journal of Advertising Research 35, 63–68.

Mustafa, M., Taib, M.N., Haji Murat, Z., Sulaiman, N.B., Mohd Aris, S.A., 2020. Classification of EEG Spectrogram Image with ANN Approach for Brainwave Balancing Application. International journal of simulation: systems, science & technology. https://doi.org/10.5013/IJSSST.a.12.05.05

Mwata-Velu, T., Avina-Cervantes, J.G., Ruiz-Pinales, J., Garcia-Calva, T.A., González-Barbosa, E.-A., Hurtado-Ramos, J.B., González-Barbosa, J.-J., 2022. Improving Motor Imagery EEG Classification Based on Channel Selection Using a Deep Learning Architecture. Mathematics 10, 2302. https://doi.org/10.3390/math10132302

Qian, Y., Chen, C., Tang, L., Jia, Y., Cui, G., 2023. Parallel LSTM-CNN Network With Radar Multispectrogram for Human Activity Recognition. IEEE Sensors Journal 23, 1308–1317. https://doi.org/10.1109/JSEN.2022.3224083

Ramos-Aguilar, R., Olvera-López, J.A., Olmos-Pineda, I., Sánchez-Urrieta, S., 2020. Feature extraction from EEG spectrograms for epileptic seizure detection. Pattern Recognition Letters 133, 202–209. https://doi.org/10.1016/j.patrec.2020.03.006

Shankar, A., Khaing, H.K., Dandapat, S., Barma, S., 2020. Epileptic Seizure Classification Based on Gramian Angular Field Transformation and Deep Learning, in: 2020 IEEE

Applied Signal Processing Conference (ASPCON). Presented at the 2020 IEEE Applied Signal Processing Conference (ASPCON), pp. 147–151. https://doi.org/10.1109/ASPCON49795.2020.9276717
Subasi, A., Tuncer, T., Dogan, S., Tanko, D., Sakoglu, U., 2021. EEG-based emotion recognition using tunable Q wavelet transform and rotation forest ensemble classifier. Biomedical Signal Processing and Control 68, 102648. https://doi.org/10.1016/j.bspc.2021.102648
Suhaimi, N.S., Mountstephens, J., Teo, J., 2020. EEG-Based Emotion Recognition: A State-of-the-Art Review of Current Trends and Opportunities. Computational Intelligence and Neuroscience 2020, e8875426. https://doi.org/10.1155/2020/8875426
Wagh, K.P., Vasanth, K., 2022. Performance evaluation of multi-channel electroencephalogram signal (EEG) based time frequency analysis for human emotion recognition. Biomedical Signal Processing and Control 78, 103966. https://doi.org/10.1016/j.bspc.2022.103966
Wang, Z., Oates, T., 2015. Encoding Time Series as Images for Visual Inspection and Classification Using Tiled Convolutional Neural Networks.
Wang, Z.-M., Hu, S.-Y., Song, H., 2019. Channel Selection Method for EEG Emotion Recognition Using Normalized Mutual Information. IEEE Access 7, 143303–143311. https://doi.org/10.1109/ACCESS.2019.2944273
Xia, K., Huang, J., Wang, H., 2020. LSTM-CNN Architecture for Human Activity Recognition. IEEE Access 8, 56855–56866. https://doi.org/10.1109/ACCESS.2020.2982225
Zhang, G., Si, Y., Wang, D., Yang, W., Sun, Y., 2019. Automated Detection of Myocardial Infarction Using a Gramian Angular Field and Principal Component Analysis Network. IEEE Access 7, 171570–171583. https://doi.org/10.1109/ACCESS.2019.2955555
Zhang, Y., Chen, J., Tan, J.H., Chen, Yuxuan, Chen, Yunyi, Li, D., Yang, L., Su, J., Huang, X., Che, W., 2020. An Investigation of Deep Learning Models for EEG-Based Emotion Recognition. Frontiers in Neuroscience 14.
Zheng, W.-L., Lu, B.-L., 2015. Investigating Critical Frequency Bands and Channels for EEG-Based Emotion Recognition with Deep Neural Networks. IEEE Transactions on Autonomous Mental Development 7, 162–175. https://doi.org/10.1109/TAMD.2015.2431497